International Journal of Biological Macromolecules 301 (2025) 140367

Contents lists available at ScienceDirect

International Journal of Biological Macromolecules

journal homepage: www.elsevier.com/locate/ijbiomac

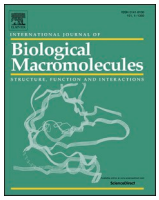

Amyloid capture and aggregation inhibition by human serum albumin

Diego Cora, Wajih Al-Soufi, Mercedes Novo *

Departamento de Química Física, Facultade de Ciencias, Campus Terra, Universidade de Santiago de Compostela, 27002 Lugo, Spain

ARTICLE INFO

Keywords:
Fluorescence
Alzheimer's disease
Amyloid
Fluorescence correlation spectroscopy
FCS
Human serum albumin
HSA
Supramolecular association
Aggregation

ABSTRACT

Alzheimer's disease (AD) is a prevalent neurodegenerative disorder characterized by amyloid-beta (Aβ) aggregation, primarily involving the peptides Aβ40 and Aβ42. Human serum albumin (HSA) has emerged as a potential therapeutic agent due to its ability to bind Aβ, inhibit aggregation, and promote disaggregation. This study quantitatively examined the interactions of HSA with both monomeric and aggregated forms of Aβ40 and Aβ42 using fluorescence techniques, including bulk steady-state fluorescence, fluorescence anisotropy, time-resolved fluorescence, and Fluorescence Correlation Spectroscopy (FCS). The binding constants determined from these methods were $4.45 \times 10^4\ M^{-1}$ for Aβ42 and $1.8 \times 10^4 M^{-1}$ for Aβ40, indicating strong but differential affinities. FCS demonstrated that HSA effectively dissociates Aβ aggregates, shifting the equilibrium toward monomeric states, with the disaggregation capacity positively correlated with HSA concentration. These findings support HSA's utility in therapies like plasma exchange to reduce the cerebral Aβ burden, providing critical insights into its mechanistic role and therapeutic potential.

1. Introduction

Alzheimer's disease (AD) is a neurodegenerative disorder currently affecting 1 in 9 people aged 65 and older, being the most common form of dementia among the elderly [1,2]. The pathogenesis of AD remains only partially understood, with the aggregation of amyloid-beta (Aβ) and tau proteins being central to current hypotheses. The amyloid cascade hypothesis posits that the accumulation of Aβ peptides in the brain initiates a series of events leading to the disease's onset [3]. Among the Aβ peptides, Aβ40 (composed of 40 amino acids) and Aβ42 (composed of 42 amino acids) are predominant, with Aβ42 being more hydrophobic and prone to aggregation [4,5].

Recent therapeutic advancements for AD include plasma exchange (PE) with albumin replacement, which leverages the interaction between human serum albumin (HSA) and amyloid-beta peptides [6,7]. It has been observed that a critical aspect of AD pathogenesis is the impaired clearance of Aβ in the brain [8,9]. Since approximately 90 % of plasma Aβ is bound to HSA, with only a small fraction remaining free [10], replacing the patient's Aβ-carrying HSA with free HSA during PE facilitates the elimination of Aβ from the brain through the blood-brain barrier (BBB) by an equilibrium shift [11]. In this way the Aβ burden can be reduced in the brain. This therapeutic approach is utilized in the AMBAR (Alzheimer Management by Albumin Replacement) project developed by Grifols [12].

Additionally, HSA is known to inhibit Aβ self-association [13–15] and promote the disassembly of aggregated Aβ fibrils, although this inhibition may be reduced in the presence of fatty acids [16,17], or enhanced by the presence of other compounds like serotonin, that promote the interaction with Aβ monomers [18], potentially affecting treatment efficacy. Experimental and computational studies consistently identify domain III of HSA, particularly residues 494–515 in the C-terminal region, as critical for binding Aβ peptides [15,19–21]. This region aligns closely with the central hydrophobic core of Aβ, a domain essential for Aβ self-association. Hydrophobic interactions primarily drive this binding [19]. These interactions disrupt β-sheet formation in Aβ and favoring α-helical conformations, thereby reducing aggregation propensity [20,21].

Although HSA shows therapeutic potential in AD, the precise mechanisms involved are not fully understood. Despite numerous studies investigating HSA's interaction with amyloids through various experimental and computational techniques, consensus on the interaction strength and its impact on disaggregation has yet to be reached. As summarized in Table 1, prior studies on these interactions have yielded inconsistent results, likely due to the complexity of the Aβ aggregation process and challenges in accurately quantifying these processes.

This study aims to comprehensively investigate the interactions between HSA and both monomeric and aggregated forms of Aβ42 and Aβ40. Specifically, our objectives are to determine whether HSA binds to

* Corresponding author.
E-mail address: m.novo@usc.es (M. Novo).

https://doi.org/10.1016/j.ijbiomac.2025.140367
Received 1 December 2024; Received in revised form 22 January 2025; Accepted 25 January 2025
Available online 27 January 2025

Table 1
Summary of published studies on the interactions between Aβ42, Aβ40, and HSA.

Reference	Year	Qualitative or quantitative information	Technique
Kuo et al. [22]	2000	Apparent 1:1 stoichiometry for both monomeric Aβ peptides.	Immunoassays
Rózga et al. [23]	2007	$K = (2.1 \pm 0.6) \times 10^5\ M^{-1}$ for Aβ40.	CD
Milojevic et al. [24]	2009	No interaction with monomeric Aβ but with the oligomers.	NMR
Costa el at [25].	2012	$K = (1.72 \pm 0.24) \times 10^6\ M^{-1}$ for Aβ42.	SPR & Immunoassays
Stanyon et al. [26]	2012	$K = 2 \times 10^5\ M^{-1}$ for both monomeric Aβ peptides.	Fluorescence & TEM
Algamal et al. [19]	2013	K_D with Aβ oligomers in the sub-μM range.	Fluorescence & NMR
Algamal et al. [27]	2017	$K = 0.1–1 \times 10^4\ M^{-1}$ for Aβ40 and weaker interaction for Aβ42.	NMR

these amyloid species and whether this interaction facilitates the disaggregation of preformed Aβ aggregates, advancing the quantitative understanding of these interactions and their implications for the PE treatment. Additionally, we aim to develop a mechanistic model for HSA's role in amyloid disaggregation and assess its efficacy in capturing and disaggregating amyloid aggregates, in alignment with the therapeutic framework proposed by the AMBAR project.

To explore these interactions, we conducted titration experiments with fluorescently N-terminally labelled Aβ42* and Aβ40*, in both monomeric and aggregated states. These experiments employed bulk steady-state fluorescence, anisotropy, and time-resolved fluorescence techniques, as well as Fluorescence Correlation Spectroscopy (FCS) at the single-molecule level.

Our research group has also previously analysed amyloid aggregation, identifying the critical aggregation concentration at which aggregates begin to form and characterizing the morphology and composition of Aβ40 and Aβ42 aggregates. This knowledge provides the foundation for interpreting the results presented here [28,29].

2. Results and discussion

The interaction between amyloid peptides and serum albumin can be studied using steady-state and time-resolved fluorescence techniques, as well as FCS, by monitoring changes in specific properties upon association, such as quantum yield, spectral shift, anisotropy, fluorescence lifetime, and diffusion coefficient. These techniques also provide insights into the number of fluorescent species and their mobility, making them powerful tools to investigate processes like amyloid self-aggregation and its association with HSA.

In this study, series of emission spectra, fluorescence anisotropy, fluorescence intensity decays and fluorescence correlation curves of labelled amyloids - Aβ42* and Aβ40* (in both monomeric and aggregated states) - were measured in the presence of varying concentrations of HSA. These measurements provided insights into their interactions, allowing for the determination of the binding constant, *K*.

The proposed general association scheme with a 1:1 stoichiometry would be:

$$G^* + H \underset{k_-}{\overset{k_+}{\rightleftarrows}} C^* \quad (1)$$

where G* refers to a fluorescent guest molecule, in this case the guest peptides Aβ42* or Aβ40*, H to a host molecule, in this case the host protein HSA, and C* to the fluorescent complex formed by the two. The rate constants k_+ and k_- correspond to the association and dissociation processes, respectively, and are related to the binding equilibrium constant as follows:

$$K = k_+/k_- \quad (2)$$

2.1. Fluorescence titrations of monomeric Aβ* with HSA

Fig. 1 shows the fluorescence emission of monomeric Aβ42* and Aβ40* in the presence of different concentrations of HSA. After excitation at 488 nm, the expected fluorescent band with maximum emission around 530 nm is observed for the labelled Aβ* peptides (Fig. 1A and 1B). The addition of HSA resulted in an increase in the fluorescence intensity, reaching approximately a 3-fold enhancement for Aβ42* and a 1.5-fold enhancement for Aβ40* at high HSA concentrations, without a significant spectral shift. In both peptides, the fluorescence intensity at 530 nm exhibited a concentration-dependent response to HSA, characteristic of supramolecular association (Fig. 1C and D).

Principal component analysis (PCA) [30] of the series of emission spectra indicates in each case only two contributing fluorescent species. Global analysis (GA) [30] with the 1:1 stoichiometry model, Eq. (SI.1), fitted the entire sets of spectra satisfactorily, yielding the binding constants $K = (7.4 \pm 2.2)\ 10^4\ M^{-1}$ for Aβ42* and $K = (3.7 \pm 1.7)\ 10^4\ M^{-1}$ for Aβ40*, and the pure spectra of the free peptides and their corresponding complexes with HSA (green and blue thicker lines, respectively, in Fig. 1A and B). The pure spectra of the complexes demonstrate the intensity enhancement upon association, enabling the calculation of the luminescence ratio, q^λ, between the complex and the free guest. Values of q^λ at 530 nm were determined as 3.1 ± 0.1 for Aβ42* and 1.54 ± 0.02 for Aβ40*. The normalized pure spectra of the free peptides and the complexes overlap, corroborating the absence of spectral shift upon complexation. This outcome indicates that the fluorophore does not interfere with the complexation of the peptides.

It should be noted that the intensity values presented in Fig. 1C and D correspond to multiple measurement series with different Aβ* concentrations, some of them higher than the critical aggregation concentration (*cac*) of the peptides [28,29] (see Table SI.1). The relatively high data dispersion, likely due to strong peptide adsorption peptides to various surfaces and oligomer formation, especially in samples with low serum albumin concentrations, highlights the challenge of obtaining reproducible intensity values. This variability contributes to the high uncertainty in the derived affinity constants.

Fluorescence anisotropy spectra of monomeric Aβ42* and Aβ40* with different concentrations of HSA show systematic variations typical of association equilibria (Fig. SI.3). Although the observed changes in the anisotropy are very small, the results are consistent with the binding constants obtained from the emission spectra and indicate again that the fluorophore attached to the peptides does not interact with a binding site in the HSA, therefore not interfering with the association of the Aβ* peptides (see Supplementary Information for further details).

The interaction of monomeric Aβ peptides with HSA was also studied using time-resolved fluorescence titrations. Fluorescence intensity decays of monomeric Aβ42* and Aβ40* at varying HSA concentrations were recorded at 530 nm. The total fluorescence intensity for each HSA concentration was also derived from the integral of these fluorescence decays. Fig. 1 shows these integrated intensities along with the steady-state fluorescence intensities for both labelled amyloids, showing good agreement despite the strong data dispersion. The binding constants, obtained by fitting eq. (SI.1) to these integrated intensities, are consistent with those derived from the steady state measurements, within their high uncertainty.

Fluorescence decays were first individually fitted with a biexponential model (eq. SI.2), revealing two lifetimes, both dependent on HSA concentration (see SI). The longer lifetime (~4 ns), which accounts for over 90 % of the fluorescence intensity, increased slightly but systematically with HSA concentration, suggesting that it represents an average of two closely spaced lifetimes corresponding to free amyloid and its HSA complex. The shorter lifetime (1–2 ns) showed less systematic variation and likely represents contributions from multiple species,

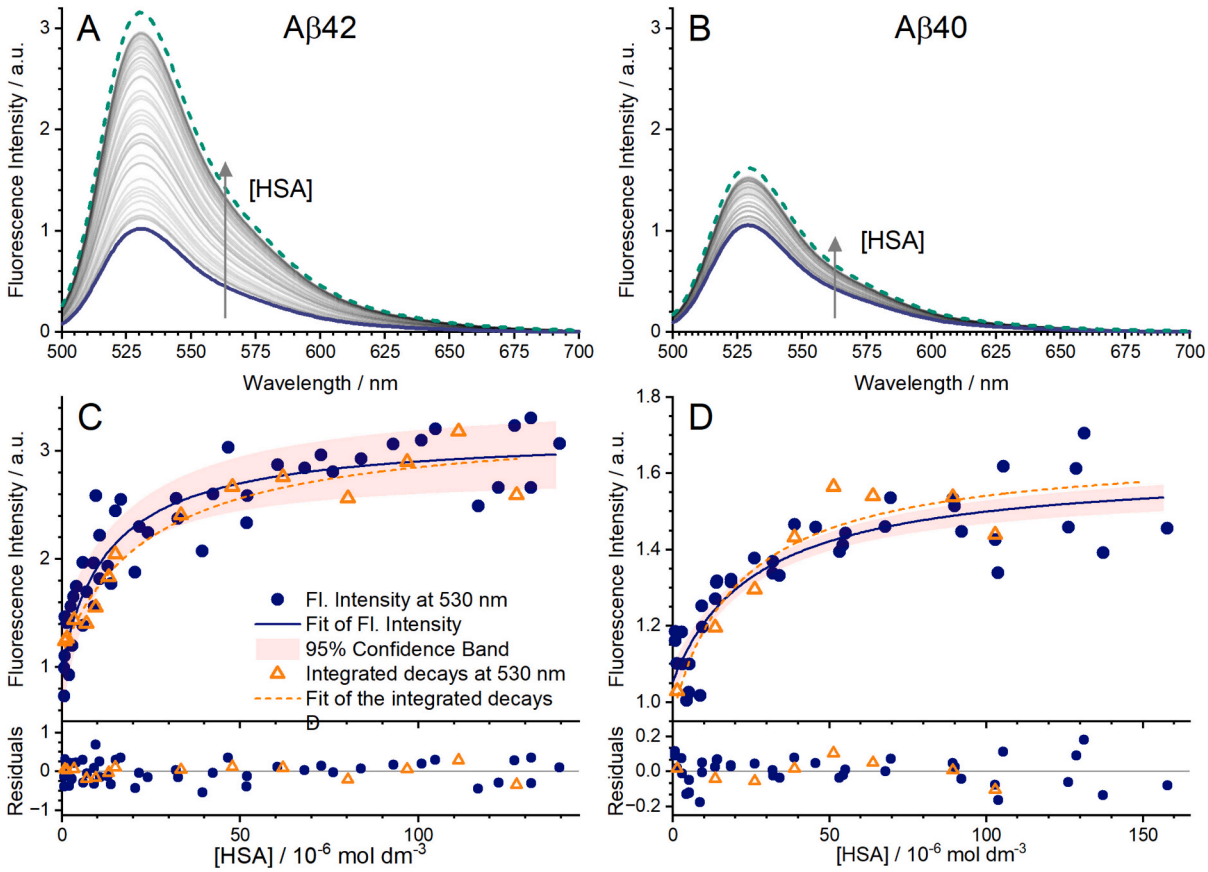

Fig. 1. A & B) Fluorescence emission spectra of monomeric Aβ42* (A) and Aβ40* (B) in presence of different concentrations of HSA, ranging from 0.5 μM to 160 μM, approximately (grey thin lines). Pure spectra obtained from GA of free guest (thick continuous line) and complex (thick dashed line) are also displayed. C & D) Steady-state fluorescence intensity values at 530 nm (dots) and integrated intensity of the fluorescence decays at 530 nm (open triangles) of monomeric Aβ42* (C) and Aβ40* (D) as a function of the HSA concentration, along with the corresponding fits, 95 % confidence band and residuals of Eq. (SI.1).

including Aβ oligomers and HSA itself (Table SI.2).

To resolve individual species lifetimes more effectively, a global analysis with a four-exponential model was applied. From this fit the fluorescence contributions (*FC*) of each lifetime were calculated (Fig. 2), allowing assignment of the obtained lifetimes (Table SI.3) as follows:

- τ_1 **(<0.4 ns):** A negligible contribution likely arising from artifacts like scattered light.
- τ_2 **(~2 ns):** Contributions from quenched fluorophore conformations in self-aggregated Aβ and HSA autofluorescence.
- τ_3 **(~3.9 ns):** Lifetime of monomeric Aβ*, decreasing with rising HSA concentration.
- τ_4 **(~4.2 ns):** Lifetime of the Aβ*-HSA complex, increasing with HSA concentration.

Fig. 2 shows that τ_3 and τ_4 dominate the fluorescence intensity for both Aβ42* and Aβ40*, supporting their assignment to free and complexed peptides, respectively. The binding constants derived from fits of a 1:1 association to these contributions were consistent with steady-state measurements, but the strong correlation between lifetimes and

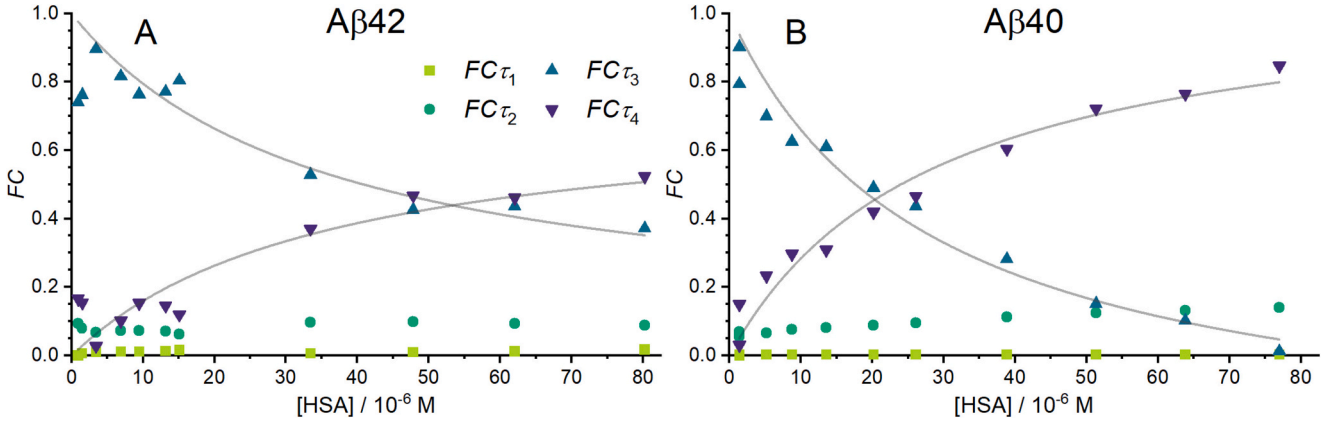

Fig. 2. Fluorescence contributions (*FC*) of the four lifetimes (Table SI.3) observed for Aβ42* (A) and Aβ40* (B) as a function of HSA concentration. The grey lines were added as guide for the eye.

amplitudes limits the precise quantification. However, the dependence on the HSA concentration of the contributions of τ_3 and τ_4 confirms a binding equilibrium, providing further evidence of Aβ-HSA association.

The results obtained from various classical fluorescence techniques clearly demonstrate the interaction between the peptides Aβ42* and Aβ40* with HSA, with the interaction being slightly weaker for Aβ40*. However, precise determination of binding constants is challenging with these techniques, as they depend on absolute fluorescence intensities. We suggest that significant peptide adsorption to surfaces and interfaces, combined with their propensity to aggregate, contributes to the high variability in the data and the resulting lack of reproducibility. These challenges are mitigated at the significantly lower peptide concentrations employed in single-molecule techniques such as FCS, as discussed in the following sections.

2.2. FCS titrations of monomeric Aβ* with HSA

To obtain a more precise determination of the binding constants of amyloids with serum albumin, FCS titrations were performed. In these experiments, complexation was monitored through changes in the diffusion correlation time, t_D, which reflects the reduced diffusion coefficient of the amyloid peptide when it associated with the HSA. Unlike techniques reliant on absolute fluorescence intensities, this method is much less affected by issues such as peptide adsorption or aggregation.

Fluorescence correlation curves of monomeric Aβ42* and Aβ40* at varying HSA concentrations were recorded (Fig. SI.6) and fitted using Eq. (SI.5). A single diffusion time was obtained for each curve which changes systematically with HSA concentration as shown in Fig. 3. This mean diffusion time, $\bar{\tau}_D$, described by Eq. (SI.6), represents a weighted average of the diffusion times of the free amyloid and its complex with HSA. It reflects a fast-exchange regime, where the peptide transitions between free and complexed states during its transit through the observation volume. Fitting Eq. (SI.6) to the experimental values yielded diffusion correlation times for free peptides and their complexes, along with the binding constants: $K = (4.45 \pm 0.03) \times 10^4\ M^{-1}$ for Aβ42* and $K = (1.8 \pm 0.5) \times 10^4\ M^{-1}$ for Aβ40*.

The translational diffusion coefficients (D) and hydrodynamic radii (R_H) were also determined for the monomeric Aβ* peptides and their complexes (Eqs. (SI.7) and (SI.8)). Additionally, the shape index (ν), which provides information about the shape of the diffusing particle, ($\nu = 1/3$ for homogeneous spheres, $\nu = 1/2$ for random coils, $\nu = 1$ for rigid rods), was calculated (detailed analysis given in the Supplementary Information). All results are shown in Table 2.

The limiting diffusion coefficient for the monomeric labelled peptide Aβ42* was significantly higher than that reported in our previous aggregation studies [28,29], suggesting that HSA promotes disaggregation of residual small oligomers, yielding coefficients more representative of monomeric peptides. However, for Aβ40*, the diffusion coefficient was lower than the one reported [31], what is attributed to the stronger tendency of this peptide to form small metastable oligomers, even at concentrations below its *cac* [29]. These results will be discussed in more detail below.

Table 2
Diffusional properties of the free and the complexed amyloids at 25 °C, calculated from the results of the fit of Eq. (SI.6) to the mean diffusion correlation times shown in Fig. 3.

Species	D / 10^{-10} m^2 s^{-1}	R_H / Å	ν
Aβ42*	1.7 ± 0.1	14 ± 1	0.40 ± 0.01
Aβ42*:HSA	0.81 ± 0.05	30 ± 2	0.367 ± 0.009
Aβ40*	1.4 ± 0.1	17 ± 1	0.42 ± 0.01
Aβ40*:HSA	1.19 ± 0.08	21 ± 1	0.332 ± 0.009

The shape indices (ν) of the free peptides exceeds significantly the value of 1/3 expected for homogeneous spheres, indicating a less compact structure trending toward random coil conformations. These values are consistent with those reported by Danielsson et al. [31] (ν = 0.44) for a series with increasing molar mass of amyloid peptides.

For the Aβ42*-HSA complex, the diffusion coefficient matched perfectly the one reported by Kusova et al. for HSA under similar conditions ($D = (0.78 \pm 0.04) \times 10^{-10}$ m^2 s^{-1}) [32]. The hydrodynamic radius also coincides with the one calculated for native folded proteins from the number of residues of the polypeptide chain N ($R_H = (4.75 \pm 1.11$ Å$)N^{(0.29\pm0.02)} = (30 \pm 1)$ Å [33]. The shape index suggests a slight variation from a homogeneous sphere toward a less compact conformation. In contrast, the diffusion coefficient for the Aβ40*-HSA complex was unexpectedly high, likely reflecting the weaker binding constant of Aβ40* to HSA and its propensity to form small oligomers.

2.3. Association of monomeric Aβ* with HSA

The binding constants determined by the various techniques are consistent, but those derived from absolute fluorescence intensity measurements show significant uncertainties. These uncertainties may arise from aggregation and adsorption artifacts, which are undetectable by fluorescence intensity alone and can distort the results, leading to highly dispersive data.

We report the binding constants derived from FCS (Table 3), as it provides the most reliable measurement for this system. FCS is particularly well-suited for monitoring aggregation processes and association events in solution, distinguishing between monomeric and aggregated

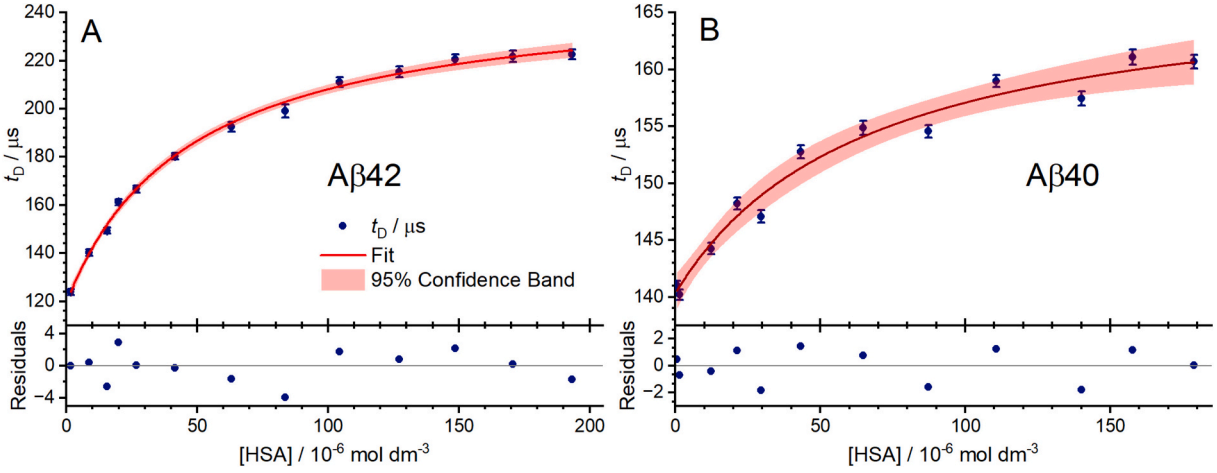

Fig. 3. Mean diffusion correlation times of monomeric Aβ42* (A) and Aβ40* (B) at HSA concentrations from 0.5 µM to 200 µM, with fits of Eq. (SI.6), 95 % confidence intervals, and residuals.

Table 3
Binding and dissociation equilibrium constants for the association of monomeric Aβ42 and Aβ40 with HSA.

Species	K / 10^4 M^{-1}	K_D / 10^{-6} M
Aβ42	4.45 ± 0.03	22.5 ± 0.2
Aβ40	1.8 ± 0.5	55 ± 14

species. This capability allows for accurate quantification of binding interactions, without interference from concentration variations of the labelled peptide that affect bulk fluorescence techniques.

The binding constants for the peptides with HSA deviate from previously reported values, positioning them between the extremes documented in the literature (Table 1). Nevertheless, the results confirm a strong interaction with a 1:1 association stoichiometry [22].

When comparing the affinity constants of the two peptides, the value for Aβ42 is approximately twice that of Aβ40. This difference can be attributed to the binding dynamics of the association process, which is related to the equilibrium constant as described by eq. (2). Although no direct dynamic information could be derived from the FCS experiments, previous studies on supramolecular association dynamics suggest that the magnitude of the affinity constant is mainly determined by the dissociation rate constant, which depends on the specific interactions between the host and the guest [34]. For Aβ42, these interactions are likely stronger due to its higher hydrophobicity, resulting in a lower dissociation rate constant. Assuming similar association rate constants for both peptides with HSA, the equilibrium constant would therefore be higher for Aβ42.

Using the binding constants from Table 3 and considering the typical HSA concentration in the plasma of healthy humans (450–680 μM) [35], approximately 96 % of Aβ42 and 92 % of Aβ40 are estimated to be bound to HSA. While this calculation does not account for the potential influence of other plasma components that might interact with or compete for amyloids, these high binding ratios highlight the strong affinity of HSA for amyloid peptides and reinforce its role as an effective amyloid carrier in PE therapy. This result can be extended to natural solutions such as blood serum or cerebrospinal fluid, although quantitative variations in binding constants may occur due to competitive interactions in these complex biological environments.

2.4. The role of Hsa in the disaggregation process of Aβ peptides

Fluorescence intensity correlation curves of aggregated Aβ42 and Aβ40 samples with varying HSA concentrations were collected. In these samples, the total amyloid concentration was maintained well above the *cac* of the peptide, corresponding to aggregation degrees around 60 % for Aβ42 and 10 % for Aβ40 [28,29]. This total Aβ concentration, with a small amount of the labelled Aβ*, was kept constant to ensure the same degree of aggregation in all samples, while the HSA concentration was varied (details in Supplementary Information).

The FCS curves (Fig. SI.7) were analysed using a Maximum Entropy Method (MEM)-based data-fitting algorithm to obtain continuous diffusion time distributions (eq. (SI.11)). The resulting distributions are presented in Fig. 4, with the diffusion times at the distribution maxima and their corresponding probabilities listed in Table 4.

In the presence of small amounts of HSA (continuous blue curve in Fig. 4A and B), both peptides show two distinct maxima in the diffusion-time distributions: a shorter diffusion-time peak at 120–140 μs and a peak at longer times around 1000 μs. The shorter diffusion-time peak matches perfectly the diffusion time of the monomer observed in Fig. 3 at the lowest HSA concentration. For Aβ40, this peak is broader and slightly shifted toward longer diffusion times compared to Aβ42, suggesting the formation of small oligomers, such as dimers or trimers, as indicated by its lower-than-expected diffusion coefficient (Table 2). The longer diffusion-time peak corresponds to peptide oligomers, consistent with previous aggregation studies [28,29].

The addition of HSA systematically altered these distributions (dashed and dotted curves in Fig. 4). The shorter diffusion-time peak shifts toward slightly higher diffusion times, reflecting the complexation of monomers with HSA. Simultaneously, the amplitude of the longer diffusion-time peaks decreases, indicating a reduction in the population of Aβ aggregates due to the disaggregation facilitated by HSA. These changes demonstrate the inhibitory role of HSA in Aβ aggregation [20,21] and support the reversibility of the oligomerization process, corroborating previous findings for Aβ40 [29].

For Aβ42 (Fig. 4A), the distribution associated with oligomers clearly decreases in amplitude as the HSA concentration increases, providing strong evidence of aggregate disassembly. Additionally, this distribution becomes broader and shifts toward shorter diffusion times, suggesting a reduction in aggregate size and an increase in polydispersity due to the HSA interactions. While these observations support the disaggregating effect of HSA, further data would be needed to confirm the hypothesis of size reduction and increased polydispersity. However, no changes were observed in the aggregate distributions that would indicate oligomer complexation by HSA, which would manifest as an increase in diffusion time. This observation strongly supports the interpretation that HSA promotes disaggregation rather than forming stable complexes with Aβ oligomers.

In contrast, for Aβ40 (Fig. 4B), oligomers are observed only at the lowest HSA concentration, and are present at significantly lower amplitudes compared to the monomer, consistent with the low degree of aggregation in these samples.

Notably, for Aβ42, the shift in monomer diffusion time upon complexation does not correspond to that observed in the titrations of monomeric samples (Fig. 3A) and remains far from the expected upper limit for the complex. This behaviour can be explained by the

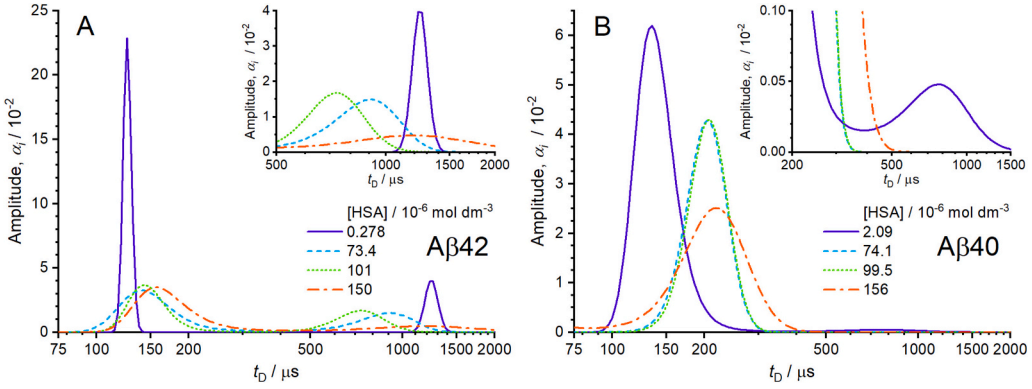

Fig. 4. Diffusion-time distributions obtained from MEM–FCS analysis (eq. (SI.11)) of the correlation curves for aggregated solutions of Aβ42 (A) and Aβ40 (B) with different concentrations of HSA.

Table 4
Diffusion times at the maxima and amplitudes of the MEM distributions obtained for the aggregated samples of Aβ42 and Aβ40 with different concentrations of HSA, corresponding to monomer-complex and oligomer diffusion. The ratio of the amplitudes between monomer-complex and oligomers is given to facilitate comparison.

	Aβ42					Aβ40				
		Amplitude at (HSA / 10^{-6} mol dm^{-3})					Amplitude at (HSA / 10^{-6} mol dm^{-3})			
	t_D / μs	0.278	73.4	101	150	t_D / μs	2.09	74.1	99.5	156
Mon-Complex	126–158	0.23	0.032	0.037	0.035	135–218	0.062	0.043	0.043	0.025
Oligomers	725–1230	0.040	0.015	0.017	0.0047	774	0.0005	–	–	–
Ratio (M-C/O)		5.7	2.2	2.2	7.4		130	–	–	–

competition between monomer complexation with HSA, which increases diffusion time, and disaggregation, which raises the concentration of monomers with shorter diffusion times. The distributions observed at shorter diffusion times likely represent weighted averages of the diffusion times for the monomer and the complex, proportional to their respective concentrations in the sample.

Instead, the diffusion time observed for the complex between Aβ40 and HSA in this analysis is consistent with the expected value, in contrast to the diffusion time obtained during the titration experiment (Fig. 3B). This discrepancy is likely due to partial aggregation of the Aβ40 sample during titration, where the presence of metastable aggregates may have influenced the diffusion times observed in the titration. As the complex with HSA forms, the system likely undergoes an equilibrium shift, leading to the dissociation of these aggregates and the formation of monomers. Complexation and monomerization exert opposite effects on the mean diffusion time. This interpretation is consistent with previous findings in the literature [36] and aggregation studies conducted in our group [29], which demonstrate that Aβ40 tends to form metastable aggregates at low concentrations, supporting the hypothesis that aggregation influences the diffusion results.

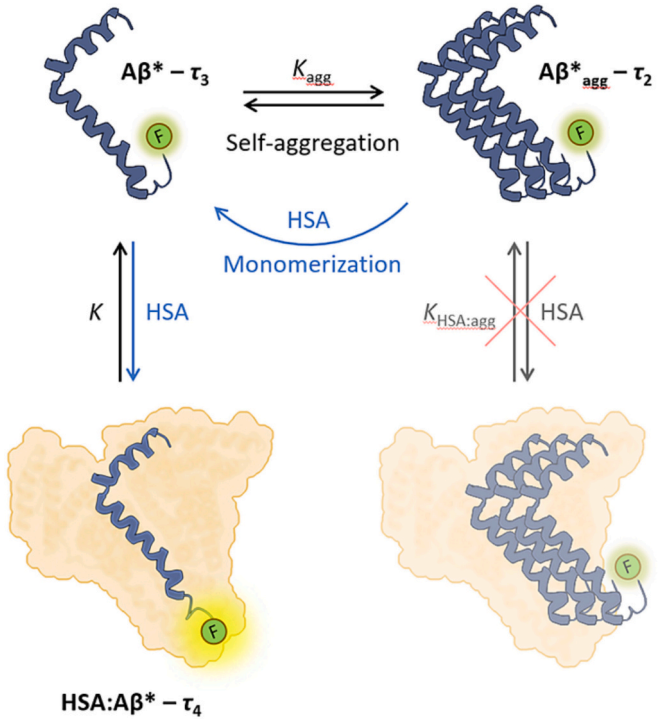

Fig. 5. Illustration of the proposed model for the association process of monomeric amyloid peptides with HSA and its role in the disaggregation process. The fluorophore, attached at the N-terminus, is half as fluorescent in the oligomers compared to the monomers, while its brightness increases upon complexation with HSA. The lifetimes assigned to the different fluorescent species are also indicated. Representations were taken from the PDB structures of Aβ42 (1IYT) and HSA (1AO6).

Based on the above discussion, a qualitative model for HSA's role in amyloid disaggregation is illustrated in Fig. 5, with lifetimes assigned to the different species. Our results suggest that the binding constant for HSA's association with monomeric Aβ peptides is significantly higher than its binding constant with Aβ aggregates $K_{HSA:agg}$ ($K > K_{HSA:agg}$), as no direct interaction with aggregated peptides was observed. This indicates that HSA functions as a monomer stabilizer, inhibiting aggregation or promoting monomer formation from preformed aggregates via an equilibrium shift. This mechanism contrasts with the 'Monomer-Competitor' model proposed by Milojevic et al. [24], which suggests that HSA binds only to aggregates to inhibit fibrillization. Additionally, for this hypothesis to hold, K must be comparable to the aggregation binding constant ($K \sim K_{agg}$).

These results align with the therapeutic mechanism proposed by the AMBAR project, where HSA facilitates Aβ clearance by promoting disaggregation rather than directly binding to existing aggregates. Since aggregates cannot cross the blood-brain barrier (BBB) but the monomeric Aβ can, the amyloid capture by HSA in the BBB surroundings would induce an equilibrium shift in the cerebrospinal fluid (CSF), leading to the dissolution of the aggregates in the patient's brain.

In contrast to previous studies summarized in Table 1, the FCS technique used in this work allows us to clearly distinguish the interaction between monomeric Aβ and HSA from aggregation effects while providing direct evidence of HSA's ability to disaggregate oligomers and small aggregates – recognized as the primary neurotoxic species in AD [37], highlighting the therapeutic relevance of plasma exchange treatment. While Kuo et al. [22] aligns with our findings on monomer-HSA interactions, other studies, such as those by Rózga et al. [23], Milojevic et al. [24], Costa et al. [25], Stanyon et al. [26], and Algamal et al. [19,27], primarily focus on conditions with high Aβ concentrations that promote aggregate and fibrillar formation, obscuring monomer-specific interactions. Additionally, various of these studies rely on ThT fluorescence, which selectively detects fibrils or highly aggregated species [38], but fails to capture clinically relevant oligomers.

Our study provides direct evidence of HSA's capacity for disaggregation, resolves inconsistencies, addresses gaps in the literature regarding the interaction between monomeric Aβ and HSA, and proposes a mechanistic role for HSA in plasma exchange treatment.

3. Conclusions

This study advances the understanding of human serum albumin interactions with amyloid-beta peptides, determining the binding affinity of the monomers and elucidating its role in promoting Aβ disaggregation. These findings hold significant implications for Alzheimer's disease research and therapy. The key conclusions are as follows:

1. **Binding affinity:** HSA binds to Aβ42 and Aβ40 with affinities of $4.45 \times 10^4 M^{-1}$ and $1.8 \times 10^4 M^{-1}$, respectively, with a 1:1 stoichiometry. The higher affinity for Aβ42 aligns with its higher hydrophobicity and stronger propensity for aggregation.
2. **Reversibility of Aggregation**: Aβ oligomers are in dynamic equilibrium with monomers, demonstrating the reversible nature of the oligomerization.

3. **Therapeutic mechanism:** HSA facilitates the disaggregation of preformed Aβ aggregates, driven by an equilibrium shift. This property highlights its efficacy in plasma exchange treatments aimed at mitigating the Aβ burden in the brain.
4. **Experimental insight:** Single-molecule techniques, such as fluorescence correlation spectroscopy, effectively addressed challenges in reproducibility caused by Aβ adsorption and aggregation. These approaches enabled precise quantification of binding constants and resolved inconsistencies reported in previous studies.

The determined HSA binding affinities and disaggregation efficiencies provide a promising foundation for optimising the efficacy of plasma exchange therapy in amyloid clearance. However, significant challenges remain in translating these findings into in vivo systems, particularly due to potential interference from other plasma components that could affect Aβ-HSA interactions. Additionally, while fluorescent labelling at the N-terminus of the peptide was carefully chosen to minimise artifacts, confirming these results using label-free techniques would strengthen the conclusions and eliminate any residual uncertainties associated with the labelling process.

4. Materials and methods

4.1. Materials

Human serum albumin (HSA) was purchased from Merck & Co., Inc. while HiLyte™ Fluor 488 labelled Aβ42 and Aβ40 (Aβ42* and Aβ40*) were purchased from Anaspec Inc. In both peptides the fluorophore is attached to the terminal nitrogen, so no interference from the marker in aggregation or interaction with HSA is expected [39]. Phosphate-buffered saline (PBS, pH 7.4, 12 mM phosphates, 150 mM NaCl, 3 mM KCl and ionic strength of 0.18 M) was used for the preparation of all samples to maintain physiological pH and salt concentration. All aqueous solutions were prepared using Milli-Q water.

4.2. Sample preparation

4.2.1. Aβ Monomerization

To perform the titration experiments with the Aβ samples, established disaggregation protocols were followed. Initially, the peptides were dissolved in hexafluoroisopropanol (HFIP) at a concentration of approximately 1 mg/mL. This organic solvent dissolves and monomerizes the peptides. Subsequently, the peptides were incubated for 1 h with occasional mixing and then shaken for about 20 min. The resulting solution was divided into several vials and evaporated using a stream of nitrogen. These vials were then placed in a desiccator, and vacuum was applied for 3 h or more to remove the remaining HFIP. The resulting dried aliquots of monomeric Aβ* peptides were stored at −20 °C [40,41].

4.2.2. Samples of monomeric Aβ with HSA

Stock solutions of Aβ* peptides were prepared by reconstituting the dried aliquots obtained in the monomerization process with PBS to achieve the target amyloid concentration and adding a certain volume of a solution of HSA to prevent amyloid adsorption and aggregation. To avoid adsorption-related artifacts, the stock solutions were gently mixed and transferred to new vials. After 20 min, the stock solution was aliquoted into several vials. Then, certain volumes of PBS or a solution of HSA were added to each vial to achieve the desired concentrations of both the HSA and the corresponding Aβ* peptide. See the sample preparation schematic in the Supplementary Information (Fig. SI.1). The Aβ* concentration was maintained constant across all samples. Any deviations were corrected afterwards in the fluorescence intensity.

We found that adding a minimal amount of HSA (5 to 10 μM) to the Aβ* stock solutions significantly improved the reproducibility in experimental conditions, particularly in steady-state and time-resolved fluorescence experiments at higher Aβ concentrations where aggregation cannot be directly monitored.

The nominal amyloid concentrations used in each titration experiment are listed in Table SI.1. For Aβ40*, the concentration was maintained below its critical aggregation concentration (*cac*) of 0.5 ± 0.3 μM, as previously determined by our group [29]. In contrast, the concentration of Aβ42* exceeded its *cac* of 90 ± 33 nM [28] in some experiments, suggesting that partial aggregation may have occurred. It is important to note that the values in Table SI.1 represent nominal Aβ* concentrations, whereas the reported *cac* values reflect true amyloid concentrations in solution, which are estimated to be at least an order of magnitude lower for Aβ42 due to its strong adsorption to surfaces [28].

4.2.3. . Samples of aggregated Aβ with HSA

Solutions of partially aggregated Aβ peptides were prepared also using the dried aliquots obtained during the monomerization process. First, the labelled monomer solution was prepared, with a specific volume of HSA solution added. This Aβ* solution was then used to reconstitute dried aliquots of unlabelled Aβ peptides, achieving a concentration above the *cac*, where aggregates form in equilibrium with the monomers. See the sample preparation schematic in the Supplementary Information (Fig. SI.2).

FCS titration experiments with HSA were performed with a constant total Aβ concentration while varying the HSA concentration. The nominal concentrations used in these experiments are given in the Supporting Information.

4.3. Experimental techniques

Steady-state fluorescence and fluorescence anisotropy spectra were recorded using an Edinburgh Instruments SF5 spectrofluorometer, with an excitation wavelength of 485 nm to match that of the FCS experiments. These experiments were conducted at room temperature around 22 °C.

Time-resolved fluorescence experiments were performed on an Edinburgh Instruments F900 spectrofluorometer employing time-correlated single photon counting. Samples were excited with a 470 nm picosecond diode laser, and intensity decays were recorded at 530 nm. Slit widths were adjusted to optimize the fluorescence signal. An adequate time interval was selected as the stop condition for the measurements in order obtain absolute intensities, which are proportional to the concentrations of the different species. The measuring temperature was also around 22 °C.

FCS measurements were performed using a custom-built FCS setup as described previously [28,29]. Details of the setup are provided in the Supporting Information. Rhodamine 123 was used to calibrate the sample volume, using a diffusion coefficient of $(4.7 \pm 0.3) \times 10^{-10}$ m^2 s^{-1} at 25 °C, based on a thorough revision of the literature [42–46]. The FCS samples were maintained at (22.0 ± 0.5) °C, but all diffusion coefficients are reported at 25 °C after correction for temperature and viscosity effects, using the Stokes-Einstein equation (see Supporting Information).

4.4. Data analysis

Both commercial and custom-made programs were employed to analyze the titration experiments using Principal Components Analysis (PCA) and nonlinear Global Analysis (GA) [47]. PCA determines the minimal number of components necessary to explain the dataset and aids in selecting an appropriate theoretical model for GA. GA performs a nonlinear fitting across the full experimental dataset using shared fit-parameters across data series to reduce parameter-correlation.

The measured properties — fluorescence intensity, anisotropy, lifetimes contributions and mean diffusion time — were modeled as functions of HSA concentration using a 1:1 association model, as described in the Supporting information. From these fits, the binding equilibrium

constant of the Aβ-HSA interaction was determined, along with the corresponding properties of the free peptides and their complexes with HSA.

The uncertainties reported for the fitted parameters correspond to the estimated statistical standard deviations of the measured quantities. For global fits of series of fluorescence data with a high number of degrees of freedom, corrections were applied to account for the non-independence of the data, avoiding the underestimation of the parameter uncertainties.

CRediT authorship contribution statement

Diego Cora: Writing – original draft, Visualization, Software, Investigation, Formal analysis, Data curation. **Wajih Al-Soufi:** Writing – review & editing, Visualization, Methodology, Formal analysis, Conceptualization. **Mercedes Novo:** Writing – review & editing, Supervision, Resources, Project administration, Methodology, Funding acquisition, Conceptualization.

Declaration of competing interest

The authors declare that they have no known competing financial interests or personal relationships that could have appeared to influence the work reported in this paper.

Acknowledgments

We thank the Spanish Ministerio de Ciencia e Innovación and the Xunta de Galicia for their financial support (PID2020-120378RB-I00, ED431B 2019/18). D.C. thanks the Xunta de Galicia for his research scholarship, “Campus de Especialización Campus Terra”. We thank Claus A.M. Seidel and Suren Felekyan for helpful discussions on the data treatment.

Appendix A. Supplementary data

Supplementary figures and data analysis procedure. Supplementary data to this article can be found online at doi: https://doi.org/10.1016/j.ijbiomac.2025.140367.

References

[1] M. Prince, A. Wimo, M. Guerchet, G.-C. Ali, Y.-T. Wu, M. Prina, World Alzheimer Report 2015, The Global Impact of Dementia. An Analysis of Prevalence, Incidence, Cost and Trends, 2015.
[2] 2023 Alzheimer’s disease facts and figures, Alzheimers Dement. 19 (2023) 1598–1695. doi:https://doi.org/10.1002/alz.13016.
[3] J. Hardy, D.J. Selkoe, The amyloid hypothesis of Alzheimer’s disease: progress and problems on the road to therapeutics, Science 297 (2002) 353–356, https://doi.org/10.1126/science.1072994.
[4] J.C. Polanco, C. Li, L.-G. Bodea, R. Martinez-Marmol, F.A. Meunier, J. Götz, Amyloid-β and tau complexity — towards improved biomarkers and targeted therapies, Nat. Rev. Neurol. 14 (2018) 22–39, https://doi.org/10.1038/nrneurol.2017.162.
[5] M. Calabrò, C. Rinaldi, G. Santoro, C. Crisafulli, The biological pathways of Alzheimer disease: a review, AIMS Neurosci. 8 (2020) 86–132, https://doi.org/10.3934/Neuroscience.2021005.
[6] M. Boada, O.L. López, J. Olazarán, L. Núñez, M. Pfeffer, M. Paricio, J. Lorites, G. Piñol-Ripoll, J.E. Gámez, F. Anaya, D. Kiprov, J. Lima, C. Grifols, M. Torres, M. Costa, J. Bozzo, Z.M. Szczepiorkowski, S. Hendrix, A. Páez, A randomized, controlled clinical trial of plasma exchange with albumin replacement for Alzheimer’s disease: primary results of the AMBAR study, Alzheimers Dement. J. Alzheimers Assoc. 16 (2020) 1412–1425, https://doi.org/10.1002/ALZ.12137.
[7] M. Boada, P. Martínez-Lage, P. Serrano-Castro, M. Costa, A. Páez, Therapeutic plasma exchange with albumin: a new approach to treat Alzheimer’s disease, Expert Rev. Neurother. 21 (2021) 843–849, https://doi.org/10.1080/14737175.2021.1960823.
[8] I. Cockerill, J.-A. Oliver, H. Xu, B.M. Fu, D. Zhu, Blood-brain barrier integrity and clearance of amyloid-β from the BBB, in: B.M. Fu, N.T. Wright (Eds.), Mol. Cell. Tissue Eng. Vasc, Syst., Springer International Publishing, Cham, 2018, pp. 261–278, https://doi.org/10.1007/978-3-319-96445-4_14.
[9] K.G. Mawuenyega, W. Sigurdson, V. Ovod, L. Munsell, T. Kasten, J.C. Morris, K. E. Yarasheski, R.J. Bateman, Decreased clearance of CNS beta-amyloid in Alzheimer’s disease, Science 330 (2010) 1774, https://doi.org/10.1126/SCIENCE.1197623.
[10] A.L. Biere, B. Ostaszewski, E.R. Stimson, B.T. Hyman, J.E. Maggio, D.J. Selkoe, Amyloid beta-peptide is transported on lipoproteins and albumin in human plasma, J. Biol. Chem. 271 (1996) 32916–32922, https://doi.org/10.1074/JBC.271.51.32916.
[11] M. Boada, P. Ortiz, F. Anaya, I. Hernández, J. Muñoz, L. Núñez, J. Olazarán, I. Roca, G. Cuberas, L. Tárraga, M. Buendia, R.P. Pla, I. Ferrer, A. Páez, Amyloid-targeted therapeutics in Alzheimer’s disease: use of human albumin in plasma exchange as a novel approach for Abeta mobilization, Drug News Perspect. 22 (2009) 325–339, https://doi.org/10.1358/dnp.2009.22.6.1395256.
[12] M. Boada, O. López, L. Núñez, Z. Szczepiorkowski, M. Torres, C. Grifols, A. Páez, Plasma exchange for Alzheimer’s disease management by albumin replacement (AMBAR) trial: study design and progress, Alzheimers Dement. Transl. Res. Clin. Interv. 5 (2019) 61–69, https://doi.org/10.1016/j.trci.2019.01.001.
[13] J. Milojevic, V. Esposito, R. Das, G. Melacini, Understanding the molecular basis for the inhibition of the Alzheimer’s Aβ-peptide oligomerization by human serum albumin using saturation transfer difference and off-resonance relaxation NMR spectroscopy, J. Am. Chem. Soc. 129 (2007) 4282–4290, https://doi.org/10.1021/ja067367+.
[14] J. Milojevic, G. Melacini, Stoichiometry and affinity of the human serum albumin-Alzheimer’s Aβ peptide interactions, Biophys. J. 100 (2011) 183–192, https://doi.org/10.1016/j.bpj.2010.11.037.
[15] P. Picón-Pagès, J. Bonet, J. García-García, J. Garcia-Buendia, D. Gutierrez, J. Valle, C.E.S. Gómez-Casuso, V. Sidelkivska, A. Alvarez, A. Perálvarez-Marín, A. Suades, X. Fernàndez-Busquets, D. Andreu, R. Vicente, B. Oliva, F.J. Muñoz, Human albumin impairs amyloid β-peptide fibrillation through its C-terminus: from docking modeling to protection against neurotoxicity in Alzheimer’s disease, Comput. Struct, Biotechnol. J. 17 (2019) 963–971, https://doi.org/10.1016/j.csbj.2019.06.017.
[16] D.C. Bode, H.F. Stanyon, T. Hirani, M.D. Baker, J. Nield, J.H. Viles, Serum Albumin’s protective inhibition of amyloid-β Fiber formation is suppressed by cholesterol, fatty acids and warfarin, J. Mol. Biol. 430 (2018) 919–934, https://doi.org/10.1016/J.JMB.2018.01.008.
[17] C. Guo, H.X. Zhou, Fatty acids compete with Aβ in binding to serum albumin by quenching its conformational flexibility, Biophys. J. 116 (2019) 248–257, https://doi.org/10.1016/J.BPJ.2018.11.3133.
[18] E.A. Litus, A.S. Kazakov, E.I. Deryusheva, E.L. Nemashkalova, M.P. Shevelyova, A. A. Nazipova, M.E. Permyakova, E.V. Raznikova, V.N. Uversky, S.E. Permyakov, Serotonin promotes serum albumin interaction with the monomeric amyloid β peptide, Int. J. Mol. Sci. 22 (2021) 5896, https://doi.org/10.3390/ijms22115896.
[19] M. Algamal, J. Milojevic, N. Jafari, W. Zhang, G. Melacini, Mapping the interactions between the Alzheimer’s Aβ-peptide and human serum albumin beyond domain resolution, Biophys. J. 105 (2013) 1700, https://doi.org/10.1016/J.BPJ.2013.08.025.
[20] T.S. Choi, H.J. Lee, J.Y. Han, M.H. Lim, H.I. Kim, Molecular insights into human serum albumin as a receptor of amyloid-β in the extracellular region, J. Am. Chem. Soc. 139 (2017) 15437–15445, https://doi.org/10.1021/jacs.7b08584.
[21] H. Xie, C. Guo, Albumin alters the conformational Ensemble of Amyloid-β by promiscuous interactions: implications for amyloid inhibition, Front. Mol. Biosci. 7 (2021), https://doi.org/10.3389/fmolb.2020.629520.
[22] Y.-M. Kuo, T.A. Kokjohn, W. Kalback, D. Luehrs, D.R. Galasko, N. Chevallier, E. H. Koo, M.R. Emmerling, A.E. Roher, Amyloid-β peptides interact with plasma proteins and erythrocytes: implications for their quantitation in plasma, Biochem. Biophys. Res. Commun. 268 (2000) 750–756, https://doi.org/10.1006/bbrc.2000.2222.
[23] M. Rózga, M. Kłoniecki, A. Jabłonowska, M. Dadlez, W. Bal, The binding constant for amyloid Abeta40 peptide interaction with human serum albumin, Biochem. Biophys. Res. Commun. 364 (2007) 714–718, https://doi.org/10.1016/J.BBRC.2007.10.080.
[24] J. Milojevic, A. Raditsis, G. Melacini, Human serum albumin inhibits Aβ fibrillization through a “monomer-competitor” mechanism, Biophys. J. 97 (2009) 2585–2594, https://doi.org/10.1016/J.BPJ.2009.08.028.
[25] M. Costa, A.M. Ortiz, J.I. Jorquera, Therapeutic albumin binding to remove amyloid-β, J. Alzheimers Dis. JAD 29 (2012) 159–170, https://doi.org/10.3233/JAD-2012-111139.
[26] H.F. Stanyon, J.H. Viles, Human serum albumin can regulate amyloid-β peptide Fiber growth in the brain Interstitium: IMPLICATIONS FOR ALZHEIMER DISEASE *, J. Biol. Chem. 287 (2012) 28163–28168, https://doi.org/10.1074/jbc.C112.360800.
[27] M. Algamal, R. Ahmed, N. Jafari, B. Ahsan, J. Ortega, G. Melacini, Atomic-resolution map of the interactions between an amyloid inhibitor protein and amyloid β (Aβ) peptides in the monomer and protofibril states, J. Biol. Chem. 292 (2017) 17158–17168, https://doi.org/10.1074/JBC.M117.792853.
[28] M. Novo, S. Freire, W. Al-Soufi, Critical aggregation concentration for the formation of early amyloid-β (1-42) oligomers, Sci. Rep. 8 (2018) 1783, https://doi.org/10.1038/s41598-018-19961-3.
[29] S. Illodo, W. Al-Soufi, M. Novo, Critical aggregation concentration and reversibility of amyloid-β (1–40) oligomers, Arch. Biochem. Biophys. 761 (2024) 110179, https://doi.org/10.1016/j.abb.2024.110179.
[30] W. Al-Soufi, M. Novo, M. Mosquera, F. Rodríguez-Prieto, Principal Component Global Analysis of Series of Fluorescence Spectra, in: Springer, NY, New York, 2011, pp. 23–45. https://link.springer.com/chapter/10.1007/978-1-4419-9672-5_2. (Accessed 29 December 2022).
[31] J. Danielsson, J. Jarvet, P. Damberg, A. Graslund, Translational diffusion measured by PFG-NMR on full length and fragments of the Alzheimer ab(1-40) peptide.

Determination of hydrodynamic radii of random coil peptides of varying length, Magn. Reson. Chem. 40 (2002) S89–S97.
[32] A.M. Kusova, A.K. Iskhakova, Yu.F. Zuev, NMR and dynamic light scattering give different diffusion information for short-living protein oligomers. Human serum albumin in water solutions of metal ions, Eur. Biophys. J. 51 (2022) 375–383, https://doi.org/10.1007/s00249-022-01605-0.
[33] D.K. Wilkins, S.B. Grimshaw, V. Receveur, C.M. Dobson, J.A. Jones, L.J. Smith, Hydrodynamic radii of native and denatured proteins measured by pulse field gradient NMR techniques, Biochemistry 38 (1999) 16424–16431, https://doi.org/10.1021/bi991765q.
[34] W. Al-Soufi, B. Reija, S. Felekyan, C.A. Seidel, M. Novo, Dynamics of supramolecular association monitored by fluorescence correlation spectroscopy, Chemphyschem Eur, J. Chem. Phys. Phys. Chem. 9 (2008) 1819–1827, https://doi.org/10.1002/cphc.200800330.
[35] M. Brandt, J. Cardinale, C. Giammei, X. Guarrochena, B. Happl, N. Jouini, T. L. Mindt, Mini-review: targeted radiopharmaceuticals incorporating reversible, low molecular weight albumin binders, Nucl. Med. Biol. 70 (2019) 46–52, https://doi.org/10.1016/j.nucmedbio.2019.01.006.
[36] B. Morel, M.P. Carrasco, S. Jurado, C. Marco, F. Conejero-Lara, Dynamic micellar oligomers of amyloid beta peptides play a crucial role in their aggregation mechanisms, Phys. Chem. Chem. Phys. 20 (2018) 20597–20614, https://doi.org/10.1039/C8CP02685H.
[37] P. Madhu, S. Mukhopadhyay, Distinct types of amyloid-β oligomers displaying diverse neurotoxicity mechanisms in Alzheimer's disease, J. Cell. Biochem. 122 (2021) 1594–1608, https://doi.org/10.1002/jcb.30141.
[38] A.A. Reinke, G.A. Abulwerdi, J.E. Gestwicki, Quantifying prefibrillar amyloids in vitro by using a "Thioflavin-like" spectroscopic method, ChemBioChem 11 (2010) 1889–1895.
[39] J.-R. Deng, N.C.-H. Lai, K.K.-Y. Kung, B. Yang, S.-F. Chung, A.S.-L. Leung, M.-C. Choi, Y.-C. Leung, M.-K. Wong, N-terminal selective modification of peptides and proteins using 2-ethynylbenzaldehydes, Commun. Chem. 3 (2020) 67, https://doi.org/10.1038/s42004-020-0309-y.
[40] W.B. Stine, K.N. Dahlgren, G.A. Krafft, M.J. LaDu, In vitro characterization of conditions for amyloid-beta peptide oligomerization and fibrillogenesis, J. Biol. Chem. 278 (2003) 11612–11622, https://doi.org/10.1074/JBC.M210207200.
[41] W.B. Stine, L. Jungbauer, C. Yu, M.J. Ladu, Preparing synthetic Aβ in different aggregation states, Methods Mol. Biol. Clifton NJ 670 (2011) 13–32, https://doi.org/10.1007/978-1-60761-744-0_2.
[42] C.T. Culbertson, S.C. Jacobson, J.M. Ramsey, Diffusion coefficient measurements in microfluidic devices, Talanta 56 (2002) 365–373.
[43] P.-O. Gendron, F. Avaltroni, K.J. Wilkinson, Diffusion Coefficients of Several Rhodamine Derivatives as Determined by Pulsed Field Gradient–Nuclear Magnetic Resonance and Fluorescence Correlation Spectroscopy, J. Fluoresc. 18 (2008) 1093–1101. doi:https://doi.org/10.1007/s10895-008-0357-7.
[44] C.B. Muller, A. Loman, W. Richtering, J. Enderlein, Dual-focus fluorescence correlation spectroscopy of colloidal solutions: influence of particle size, J. Phys. Chem. B 112 (2008) 8236–8240.
[45] Z. Petrášek, P. Schwille, Precise measurement of diffusion coefficients using scanning fluorescence correlation spectroscopy, Biophys. J. 94 (2008) 1437–1448, https://doi.org/10.1529/biophysj.107.108811.
[46] G. Majer, K. Zick, Accurate and absolute diffusion measurements of rhodamine 6G in low-concentration aqueous solutions by the PGSE-WATERGATE sequence, J. Chem. Phys. 142 (2015) 164202, https://doi.org/10.1063/1.4919054.
[47] W. Al-Soufi, M. Novo, M. Mosquera, Principal component global analysis of fluorescence and absorption spectra of 2-(2′-hydroxyphenyl)benzimidazole, Appl. Spectrosc. 55 (2001) 630–636, https://doi.org/10.1366/0003702011952253.